Journal of Geophysical Research: Space Physics

RESEARCH ARTICLE
10.1029/2018JA025365

Quasi-6-Day Wave Modulation of the Equatorial Electrojet

Yosuke Yamazaki[1], **Claudia Stolle**[1,2], **Jürgen Matzka**[1], **and Patrick Alken**[3,4]

[1]GFZ German Research Centre for Geosciences, Potsdam, Germany, [2]Faculty of Science, University of Potsdam, Potsdam, Germany, [3]Cooperative Institute for Research in Environmental Sciences, University of Colorado Boulder, Boulder, CO, USA, [4]National Centers for Environmental Information, NOAA, Boulder, CO, USA

Key Points:
- Quasi-6-day wave influence on the equatorial electrojet is revealed
- The effect depends on longitude
- The modulation of equatorial vertical plasma drift velocity can be as large as ±5.9 m/s at noon

Correspondence to:
Y. Yamazaki,
yamazaki@gfz-potsdam.de

Citation:
Yamazaki, Y., Stolle, C., Matzka, J., & Alken, P. (2018). Quasi-6-day wave modulation of the equatorial electrojet. *Journal of Geophysical Research: Physics Space Physics*, *123*, 4094–4109. https://doi.org/10.1029/2018JA025365

Received 16 FEB 2018
Accepted 3 APR 2018
Accepted article online 6 APR 2018
Published online 10 MAY 2018

Abstract The equatorial electrojet is an enhanced eastward current in the dayside *E* region ionosphere flowing along the magnetic equator. The equatorial electrojet is highly variable as it is subject to various forcing mechanisms including atmospheric waves from the lower layers of the atmosphere. There are occasionally times when the intensity of the equatorial electrojet at a fixed longitude shows an oscillatory variation with a period of approximately 6 days. We present case studies of such events based on the equatorial electrojet measurements from the CHAMP and Swarm satellites. The spatial and temporal variability of the equatorial electrojet intensity during these events reveals characteristics of a westward propagating wave with zonal wavenumber 1, consistent with the effect of the quasi-6-day planetary wave. Analyses of the geopotential height data from the Aura satellite confirm the presence of the quasi-6-day planetary wave in the lower thermosphere during the events. The amplitude of the quasi-6-day variation in the equatorial electrojet intensity depends on longitude, but no systematic longitudinal dependence is found for different events. During the event of August 2010, quasi-6-day variations are also observed by ground-based magnetometers and a radar in the Peruvian sector. The effect of the quasi-6-day wave accounts for up to ±5.9 m/s in the equatorial vertical plasma velocity at noon, which is much larger than previously predicted by a numerical model. These results suggest that the quasi-6-day planetary wave is an important source of short-term variability in the equatorial ionosphere.

1. Introduction

The *E* region of the Earth's ionosphere, at approximately 90- to 150-km altitude, is electrically conductive during the daytime, thus allowing electric currents to flow (e.g., Richmond & Maute, 2014). The dynamo action of neutral winds at middle and low latitudes generates an electromotive force to drive currents (e.g., Du & Stening, 1999; Stening, 1995). These wind-driven currents are generally not divergence free, thus resulting in a buildup of polarization charges and electric fields, which further drive currents to maintain current continuity. A consequence of this "ionospheric wind dynamo" process is the formation of the solar quiet (S_q) current system that dominates the ionospheric currents at middle and low latitudes (e.g., Chulliat et al., 2016; Takeda, 2002). Ionospheric currents near the magnetic equator have unique characteristics owing to the fact that the geomagnetic field lines are nearly horizontal, which enables the establishment of a strong vertical electric field (>10 mV/m) within ±3° from the magnetic equator (e.g., Hysell et al., 2002; Richmond, 1973; Untiedt, 1967). It is this vertical electric field that causes an amplification of the zonal current flow along the magnetic equator, and this narrow band of the enhanced current flow is called the equatorial electrojet (EEJ). Yamazaki and Maute (2017) recently reviewed the subject of S_q and EEJ.

The intensity of the EEJ varies from day to day. A part of the variability is due to the response of the equatorial electric field to geomagnetic storms and substorms (e.g., Fejer et al., 2017; Xiong et al., 2016; Yamazaki & Kosch, 2015). The EEJ variability can also arise from short-term changes in the solar extreme ultraviolet flux, which affect ionospheric conductivities. Moreover, numerical studies have shown that atmospheric waves from the lower layers of the atmosphere can make a significant contribution to the day-to-day variability of the EEJ by modulating global and local ionospheric wind dynamo processes (Kawano-Sasaki & Miyahara, 2008; Yamazaki et al., 2014). In particular, solar and lunar atmospheric tides have been identified as important sources of the day-to-day variability (e.g., Fang et al., 2013; Fuller-Rowell et al., 2010; Pedatella et al., 2012, 2016). These tidal waves, generated mainly in the troposphere and stratosphere, can propagate upward through the middle atmosphere to reach *E* region heights, where they drive electric fields and currents by the dynamo mechanism.

The climatology of atmospheric tides in the lower *E* region, 90–110 km, is now established (e.g., Forbes et al., 2008, 2013; Truskowski et al., 2014), and their climatological influence on the EEJ is well understood (e.g., Lühr & Manoj, 2013; Yamazaki et al., 2017).

Atmospheric tides are not the only kind of upward propagating wave in the Earth's atmosphere. Other types of waves that also propagate into the upper atmosphere include gravity waves, planetary waves, and Kelvin waves (e.g., Laštovička, 2006; H.-L. Liu, 2016; Oberheide et al., 2015; Yiğit & Medvedev, 2015). However, the importance of these waves for the ionospheric electrodynamics is not well understood. The present study provides observational evidence that the planetary wave with a period of ~6 days is a significant source of the day-to-day variability in the equatorial ionosphere.

Planetary waves are long-period global oscillations of the atmosphere. Observations from the middle atmosphere have revealed planetary wave signatures with periods around 2 days (e.g., Gu et al., 2013; Limpasuvan et al., 2005; Moudden & Forbes, 2014; Salby, 1981), 6 days (e.g., Forbes & Zhang, 2017; Merzlyakov et al., 2013; Pancheva et al., 2010; Talaat et al., 2001; Wu et al., 1994), 10 days (e.g., Forbes & Zhang, 2015; Hirooka & Hirota, 1984; Hirooka, 2000), and 16 days (e.g., Day et al., 2011; John & Kumar, 2016; McDonald et al., 2011). These waves travel westward, and they are generally considered as normal mode Rossby waves, which represent resonant or free oscillations of the atmosphere. The existence of such waves is predicted by the classical theory of atmospheric waves (e.g., Forbes, 1995; Longuet-Higgins, 1968).

The quasi-6-day planetary wave, or simply quasi-6-day wave, observed in the middle atmosphere is a manifestation of the first symmetric Rossby normal mode, or (1,1) mode, of the classical wave theory. This notion is supported by the facts that (1) the period of the quasi-6-day wave is close to that of the (1,1) mode, which is predicted to be ~5 days in an idealized atmosphere, (2) the quasi-6-day wave travels westward with a zonal wavenumber 1 as predicted for the (1,1) mode Rossby wave, and (3) the latitudinal structure of the quasi-6-day wave is consistent with that of the (1,1) mode. The main excitation source of the (1,1) mode Rossby wave is atmospheric heating in the troposphere due to moist convection (Miyoshi & Hirooka, 1999). Meyer and Forbes (1997) suggested that atmospheric instability in the mesosphere could also lead to the quasi-6-day wave. Talaat et al. (2002) and Lieberman et al. (2003) showed that the quasi-6-day wave in the mesosphere is mainly originated from the lower atmosphere, rather than locally driven in the mesosphere. Lieberman et al. (2003) also pointed out that the wave is strongly amplified in the mesosphere due to atmospheric instability. H.-L. Liu et al. (2004), using a general circulation model, examined how the amplification of the quasi-6-day wave in the mesosphere varies with season.

According to numerical studies (Forbes et al., 2018; Gan et al., 2016; Miyoshi, 1999; Pedatella et al., 2012), the quasi-6-day wave influence extends into *E* region heights. The interaction with tides facilitates the penetration of the quasi-6-day wave into the *E* region (Forbes et al., 2018). The neutral wind oscillation due to the quasi-6-day wave at *E* region heights is most significant over the equator. The wave amplitude in the zonal wind at the equator is predicted to be 10–30 m/s at 110 km. Miyoshi (1999) considered that the modulation of the ionospheric currents due to the quasi-6-day wave would be large enough to be detected by ground-based magnetometers. Indeed, the spectrum analysis of geomagnetic records occasionally displays a local peak around 6 days, which has often been ascribed to the quasi-6-day wave effect on the ionospheric currents (e.g., Elhawary & Forbes, 2016; Jarvis, 2006; Parish et al., 1994; Yamada, 2002). Ramkumar et al. (2009) and Gurubaran et al. (2011) presented events where ~6-day spectral peaks are detected simultaneously in the ground geomagnetic perturbations and in the mesospheric winds measured at the same site near the magnetic equator. These observations were attributed to the EEJ response to atmospheric waves from below. However, the limitation of the wave analysis at a single location is that it can reveal neither the zonal wavenumber nor the direction of the phase propagation (i.e., eastward, westward, or stationary), which is necessary for the identification of planetary waves. Pancheva et al. (2008) attempted to overcome this problem by using simultaneous measurements of the geomagnetic field at a number of low-latitude stations. They showed that during August–November 2004, the geomagnetic perturbations contained wave signals with a period of 5.75 days, propagating both eastward and westward. The westward propagating component was greater in amplitude and considered to be due to the quasi-6-day planetary wave, which was also observed in the middle atmosphere. The eastward propagating component was attributed to a Kelvin wave.

There is increasing evidence that the ionosphere is subject to the quasi-6-day wave. For instance, Takahashi et al. (2006) observed 6- to 8-day variations in the minimum virtual height of the *F* layer ($h'F$) as well

as in the zonal wind in the mesosphere and lower thermosphere (MLT) region near the equator during August–November 2004. G. Liu et al. (2010) investigated the ~6-day variation observed in the wave-4 longitudinal structure of the F_2 layer peak height (h_mF_2) during August–September 2008. They considered that these variations were caused by the ionospheric response to the eastward propagating solar diurnal tide with zonal wavenumber 3 (commonly known as DE3), which was modulated by the quasi-6-day wave observed in the MLT region. Gu et al. (2014) examined the quasi-6-day wave event of May 2003, which was identified by the temperature and wind measurements in the MLT region from the Thermosphere Ionosphere Mesosphere Energetics and Dynamics satellite. The spectrum analysis revealed the presence of a westward propagating wave with zonal wavenumber 1 not only in the temperature and winds at 100–106 km but also in the ionospheric plasma density at low latitudes derived from ground-based Global Positioning System data. The observations were attributed to the modulation of the equatorial electric field by the quasi-6-day wave that directly penetrated into the *E* region. It is known that changes in the *E* region equatorial electric field can alter the *F* region plasma density distribution through the equatorial plasma fountain effect (e.g., Rastogi & Klobuchar, 1990; Stolle et al., 2008). Gan et al. (2016, 2017), conducting an idealized simulation with the Thermosphere Ionosphere Mesosphere General Circulation Model, showed that a quasi-6-day variation is induced in the equatorial electric field during presunrise periods in response to wave forcing that mimics the quasi-6-day wave. The modulation of the equatorial electric field by the quasi-6-day wave has not been experimentally confirmed. The present study aims to fill this knowledge gap and quantify the quasi-6-day wave influence on the EEJ.

2. Data

The EEJ intensities were derived using magnetic field measurements by the absolute scalar magnetometer on board the CHAMP (Reigber et al., 2002) and Swarm (Friis-Christensen et al., 2006, 2008) satellites. Each satellite flew in a low Earth orbit with an orbital period of approximately 90 min with a high inclination angle. For each equatorial crossing on the dayside, the height-integrated EEJ intensity was retrieved from the magnetometer data based on the method described by Alken et al. (2013). Briefly, the retrieval procedures involve the removal of the core, lithospheric, and magnetospheric fields, and the separation of the residual fields into the large-scale "S_q field" and the "EEJ field" that is localized around the magnetic equator. The final step is the inversion of the EEJ field for the height-integrated EEJ current based on the Biot-Savart law. The inversion was performed under the assumption of a zonal current at 110 km directed along the magnetic equator with consideration of a realistic longitudinal dependence of declination.

It is known that variations in the EEJ magnetic field derived from the satellite data are in good agreement with the variations in ΔH derived from ground-based magnetometers (Manoj et al., 2006). Here ΔH is defined as the difference between the horizontal-component (H) geomagnetic perturbations measured near the magnetic equator and measured in the same longitude but several 100 km away from the magnetic equator. For the present study, ΔH in the Peruvian sector was obtained using the H data at Huancayo (12.05°S, 75.33°W) and Villa Remedios (16.77°S, 68.17°W). The quasi-dipole latitude (e.g., Laundal & Richmond, 2017) is 0.28° at Huancayo and −5.00° at Villa Remedios for the year 2010. The 1-min data at Huancayo are available at the INTERMAGNET website (www.intermagnet.org), and the Villa Remedios data used in this study are available at GFZ Data Services (Matzka et al., 2018).

We also used the vertical plasma drift measurements from the Jicamarca Unattended Long-term Investigations of the Ionosphere and Atmosphere (JULIA) radar (Hysell et al., 1997), located in the Jicamarca Radio Observatory (11.97°S, 76.87°W) in Peru. The JULIA V_Z data are based on observations of the vertical Doppler velocity of 150-km echoes, which move with the surrounding plasmas (Chau & Kudeki, 2006). The motion of the *F* region ionospheric plasma is dominated by the electrodynamic drift given by $\frac{\mathbf{E}\times\mathbf{B}}{|\mathbf{B}|^2}$, where **E** and **B** are the electric field and geomagnetic main field, respectively. Therefore, V_Z at the magnetic equator is a measure of the zonal electric field. In general, there is a good correlation between the day-to-day variations of ΔH and V_Z (e.g., Anderson et al., 2004).

Measurements of the geopotential height from the Microwave Limb Sounder (MLS) on the Aura satellite (Waters et al., 2006) were also used to evaluate planetary wave activity in the MLT region. Version 4.2 of the MLS geopotential height data (Schwartz et al., 2008) is available from Goddard Earth Sciences Data and Information Services Center (disc.gsfc.nasa.gov).

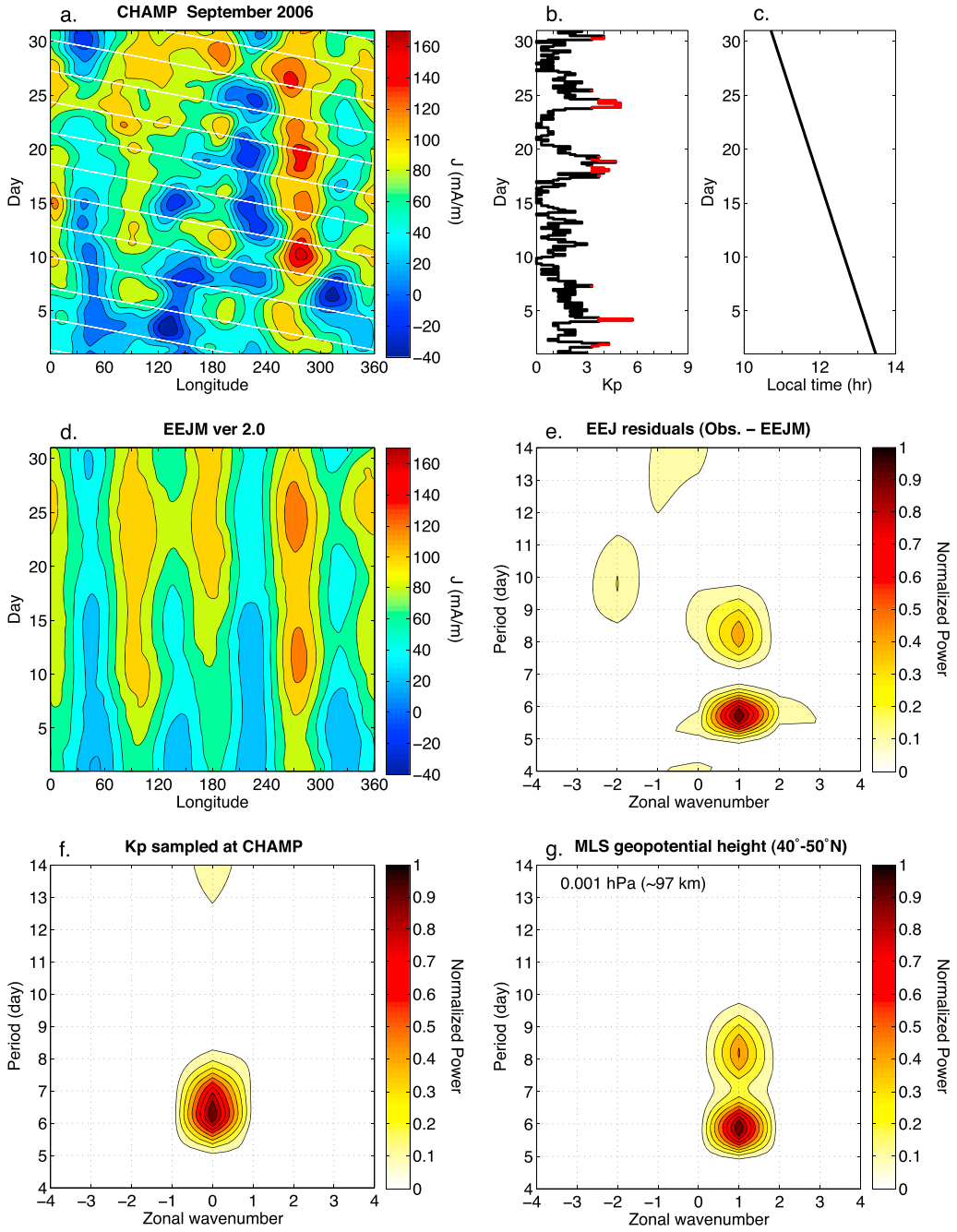

Figure 1. (a) Equatorial electrojet (EEJ) intensity during September 2006 as observed by the CHAMP satellite. The white lines represent the zero contour for the westward propagating 5.75-day wave with zonal wavenumber 1, indicating the phase propagation of the wave. (b) Geomagnetic activity index *Kp*. The red color indicates the periods of relatively high geomagnetic activity ($Kp > 3_0$). (c) Local solar time of the CHAMP measurements. (d) Same as (a) except for the empirical model, EEJM. (e) Period versus wavenumber (positive for westward propagating) spectrum for the residual equatorial electrojet intensity (observations minus EEJM predictions). The spectral power is normalized to the peak value. (f) Same as (e) except for the *Kp* index sampled at the times of the CHAMP measurements of the equatorial electrojet. These *Kp* values were analyzed as if they were variable spatially as well as temporally, according to the longitudes and times of the CHAMP measurements of the equatorial electrojet. (g) Same as (e) except for the Microwave Limb Sounder (MLS) geopotential height measurements at 0.001 hPa (~97-km height) in the latitude range 40° – 50°N by the Aura satellite.

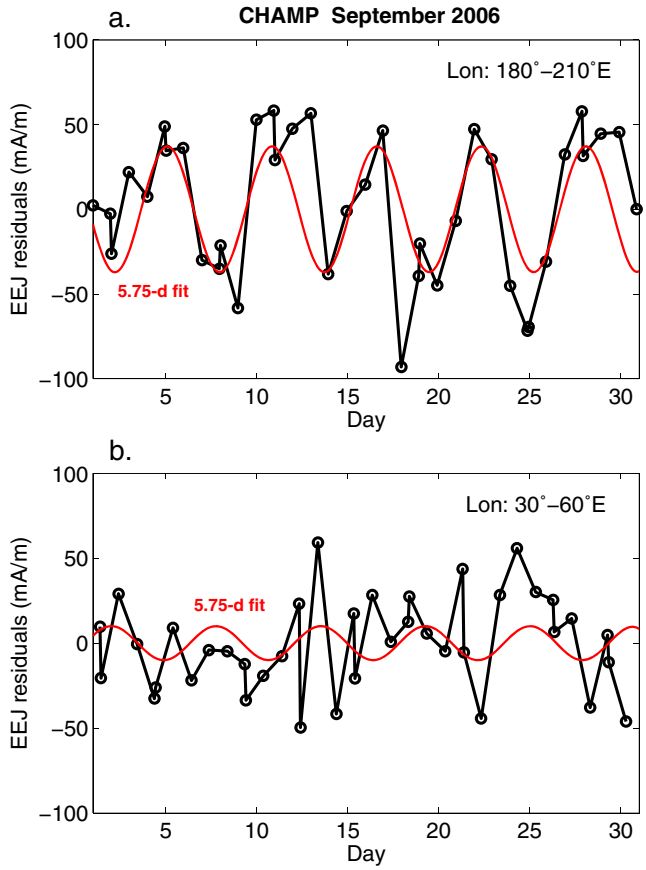

Figure 2. Equatorial electrojet (EEJ) intensity during September 2006 as observed by the CHAMP satellite at (a) 180°–210°E and (b) 30°–60°E longitudes. Also plotted in each panel is the least squares fit of the 5.75-day Fourier curve.

3. Method

We investigate the possible effect of planetary waves on the EEJ based on case studies. For each month, we plotted the EEJ intensity from CHAMP (August 2000 to August 2010) or Swarm (December 2013 to April 2017) as a function of longitude and day. Because of the highly inclined orbit of CHAMP and Swarm, the local solar time (LT) of the measurements changes only by ~3 hr in 1 month. We focus on the months when the measurements were made around 1200 LT. This is when the relative uncertainty of the measurements is smallest, as the EEJ signal is strongest during 1000–1400 LT. The monthly plot of the EEJ intensity was visually inspected, and if there is an oscillatory variation in the EEJ intensity at any longitude, the zonal wavenumber analysis described below was applied.

Following Forbes and Zhang (2017), a mathematical expression for a planetary wave is given in the form

$$A\cos\left[2\pi\left(\frac{t}{T}+s\frac{\lambda_p}{360}\right)-\phi\right], \tag{1}$$

where A is the amplitude of the wave, t is the time (in days) measured from 0000 UT of the first day of the month, T is the period of the wave (in days), s is the wavenumber, λ_p is the "pseudolongitude," which is the longitude (in degrees) subtracted by 360° times the number of Earth revolutions since the beginning of the month, and ϕ is the phase of the wave. The sign of s indicates the direction of the wave propagation. That is, $s>0$ and $s<0$ correspond to westward and eastward propagating waves, respectively, and $s=0$ represents stationary waves. The amplitude and phase of the wave can be defined for a given combination of s and T. In order to obtain a spectrum for the EEJ intensity, the power A^2 was calculated for $s=-4,-3,\cdots,4$, and for T from 4.0 to 14.0 in increments of 0.125 day. The quasi-6-day planetary wave travels westward with zonal wavenumber 1, which corresponds to $s=1$ and $T\sim 6$.

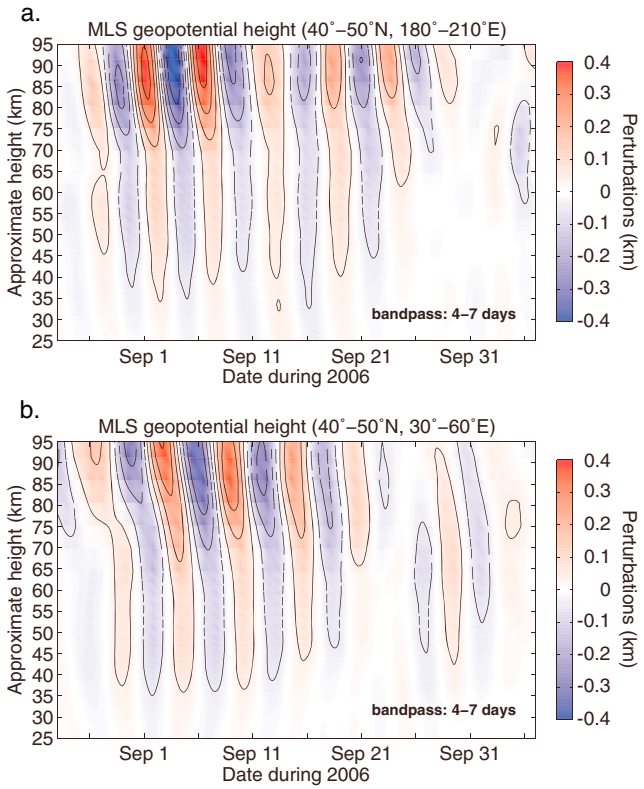

Figure 3. Quasi-6-day variations in the Microwave Limb Sounder (MLS) geopotential height extracted with a 4- to 7-day band-pass filter for (a) 180°–210°E and (b) 30°–60°E longitudes.

4. Results and Discussions

In this section, the results of the data analysis are presented for selected months, when the EEJ measurements by CHAMP or Swarm were made around noon local time and the EEJ intensity at a fixed longitude revealed an oscillatory variation with a period of approximately 6 days.

4.1. September 2006 Event

Figure 1a shows the EEJ intensity as a function of longitude and day as derived from the CHAMP data during September 2006. For the purpose of display, the data were smoothed spatially and temporally using a 3-day 30° longitude window. The short-term variability is visible over a wide range of longitudes. Especially, in the Pacific longitude sector around 120°–240°E, the EEJ intensity oscillates with a period of ~6 days. The white lines in Figure 1a indicate the phase propagation of the wave with $s = 1$ and $T = 5.75$ days, which will be shown to be the dominant wave component in the EEJ intensity during this month.

Figure 1b shows the geomagnetic activity index *Kp* during the corresponding period. The times when geomagnetic activity was relatively high (*Kp* > 3∘) are indicated by the red color. Figure 1c illustrates the local solar time for the EEJ measurements. During September 2006, the CHAMP satellite flew over the noontime sector (1030–1330 LT), where the EEJ is usually strongest.

The spatial and temporal variability of the EEJ depicted in Figure 1a can be partly explained by the effects of solar and lunar tides. Alken and Maus (2007) presented empirical models of the EEJ, EEJM. Version 2.0 of EEJM (Alken, 2009) takes into account the dependence of the EEJ intensity on the solar flux intensity, season, local solar time, longitude, and lunar time and thus is suitable for evaluating climatological solar and lunar tidal effects. Figure 1d shows the same as Figure 1a, but the results are derived from version 2.0 of the CHAMP-based EEJM. Figure 1d reveals that the wave-4 pattern dominates the longitude structure of the EEJ intensity throughout the month. The wave-4 longitude pattern is also reflected in the data (Figure 1a). The solar DE3 tide is known to be the primary cause of the wave-4 longitudinal structure in the EEJ (England et al., 2006; Lühr et al., 2008). In Figure 1d, temporal variations arise from the changes in the solar flux intensity,

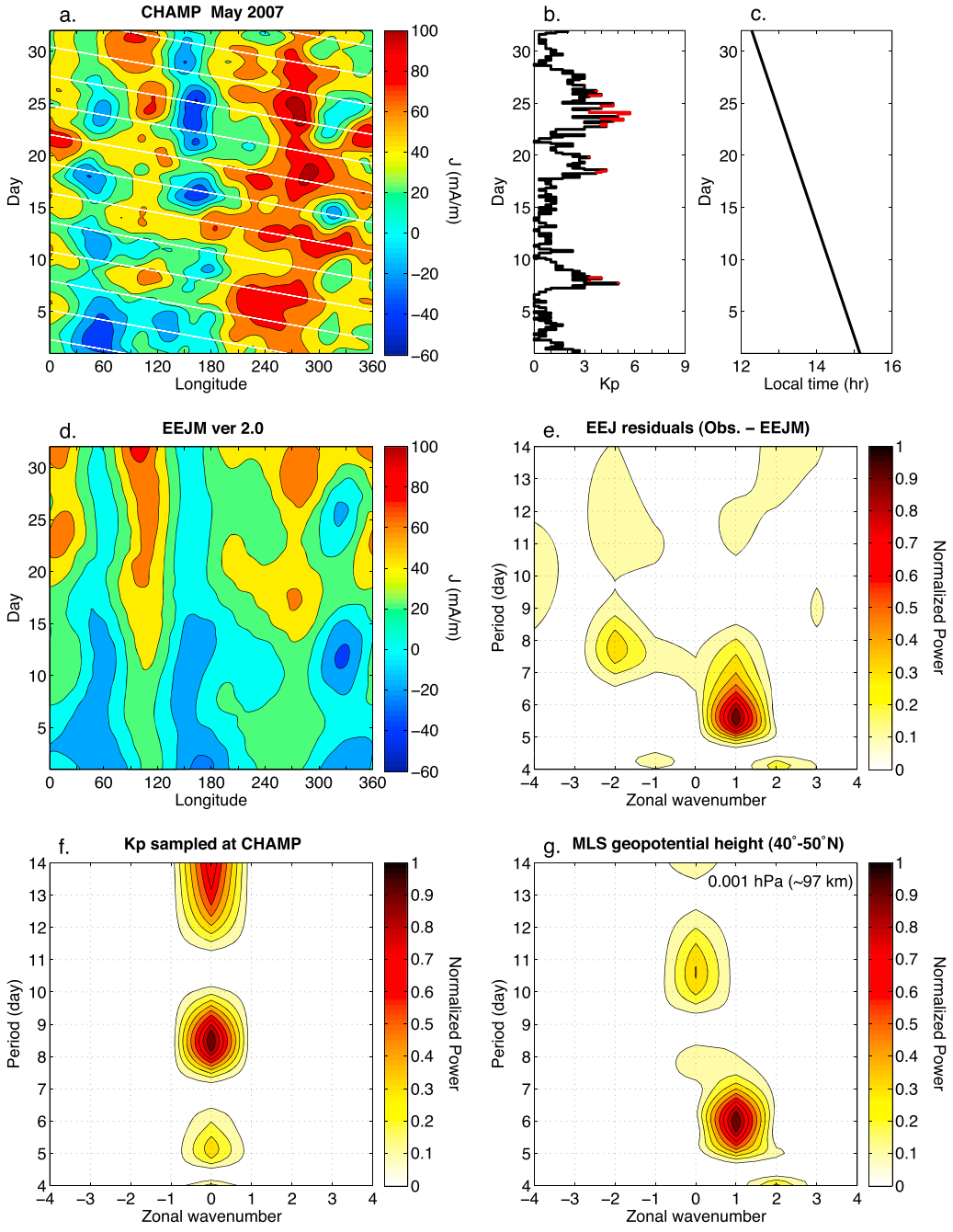

Figure 4. Similar to Figure 1 but for May 2007. The white lines in (a) represent the phase propagation of the 5.63-day wave with zonal wavenumber $s = 1$. EEJ = equatorial electrojet; EEJM = equatorial electrojet model; MLS = Microwave Limb Sounder.

season, and local solar time. It is obvious that EEJM does not reproduce the quasi-6-day oscillation that is visible in the data at some longitudes (Figure 1a).

We present in Figure 1e the spectrum for the EEJ intensity. Analyzed were the residuals of the EEJ intensity from the climatology predicted by EEJM (i.e., Figure 1a minus Figure 1d but without spatial and temporal smoothing). The spectral peak is found at the period $T = 5.75$ (± 0.10) days and zonal wavenumber $s = 1$. Thus, the observed spatial and temporal variations in the EEJ intensity are consistent with the effect that would be expected from the modulation of the electric field by the quasi-6-day planetary wave. It is also noted that the spectrum in Figure 1e has a secondary peak at $T = 8.25$ days and $s = 1$.

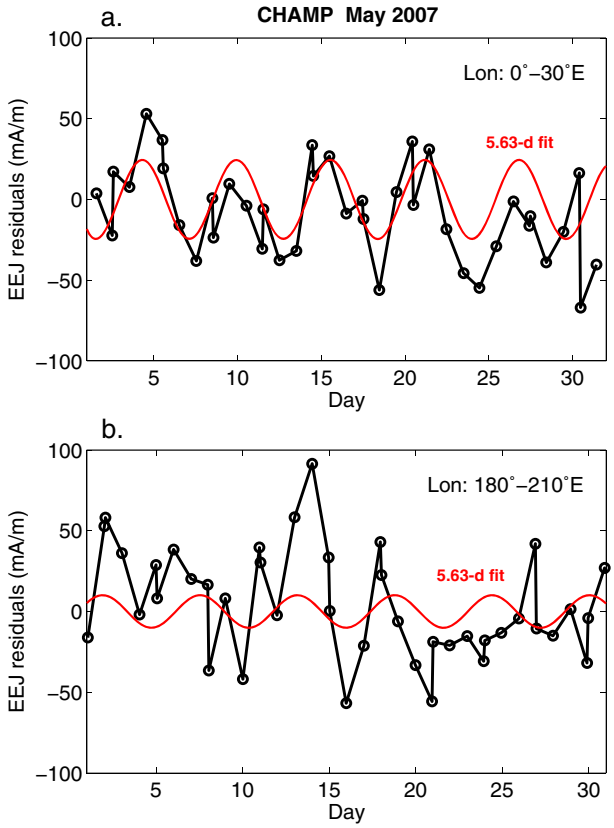

Figure 5. Equatorial electrojet (EEJ) intensity during May 2007 as observed by the CHAMP satellite at (a) 0°–30°E and (b) 180°–210°E longitudes. Also plotted in each panel is the least squares fit of the 5.63-day Fourier curve.

The EEJ variability can arise not only from atmospheric waves but also from high-latitude processes associated with geomagnetic activity. One may notice in Figure 1b that there were periods of relatively high geomagnetic activity on 18–19, 22–23, and 30 September, approximately 6 days apart from each other. Thus, it is worth considering whether the effect of such recurrent geomagnetic activity could be misinterpreted as the quasi-6-day wave effect. We address this question by sampling the *Kp* index at the times of the CHAMP measurements of the EEJ and applying the wave spectrum analysis to these *Kp* values as if they were variable spatially with longitude λ_p as well as temporally with t. Note that the *Kp* index is independent of longitude, and thus, if properly sampled, the spectrum would be dominated by the zonally symmetric component ($s = 0$). However, because of limited spatial and temporal sampling by the satellite, temporal variations in the *Kp* index can potentially alias into planetary wave spectra (i.e., s =1). It is this possibility that we are going to investigate here. Figure 1f shows the spectrum of the *Kp* index sampled at the times of the CHAMP measurements of the EEJ. The spectrum is dominated by the $s = 0$ component, with the peak period at $T \sim 6$, and there is no evidence of aliasing into the $s = 1$ component. This rules out the possibility that the spectral peak of the EEJ intensity at $s = 1$ and $T = 5.75$ days (Figure 1e) is an artifact due to zonally symmetric geomagnetic disturbances in the EEJ. A similar analysis was also performed with another geomagnetic activity index *SME*, or SuperMAG electrojet index (Newell & Gjerloev, 2011), which has a higher temporal resolution (1 min) than the *Kp* index (3 hr). The spectrum pattern for *SME* was very similar to that of *Kp* presented in Figure 1f.

Figure 1g confirms the presence of the quasi-6-day wave in the lower thermosphere during September 2006. The wave spectrum analysis was applied to the MLS geopotential height measurements at 0.001 hPa (~97 km). The result is shown for the latitude range 40°–50°N, where quasi-6-day wave activity was most prominent. We separately analyzed the data from the ascending and descending parts of the Aura orbit (corresponding to two different local time sectors). Since the results were consistent, we show in Figure 1g the average of the two. Similar results were also obtained from the measurements in the Southern Hemisphere, but the overall wave power was somewhat lower. The quasi-6-day wave in the middle atmosphere during September 2006 was

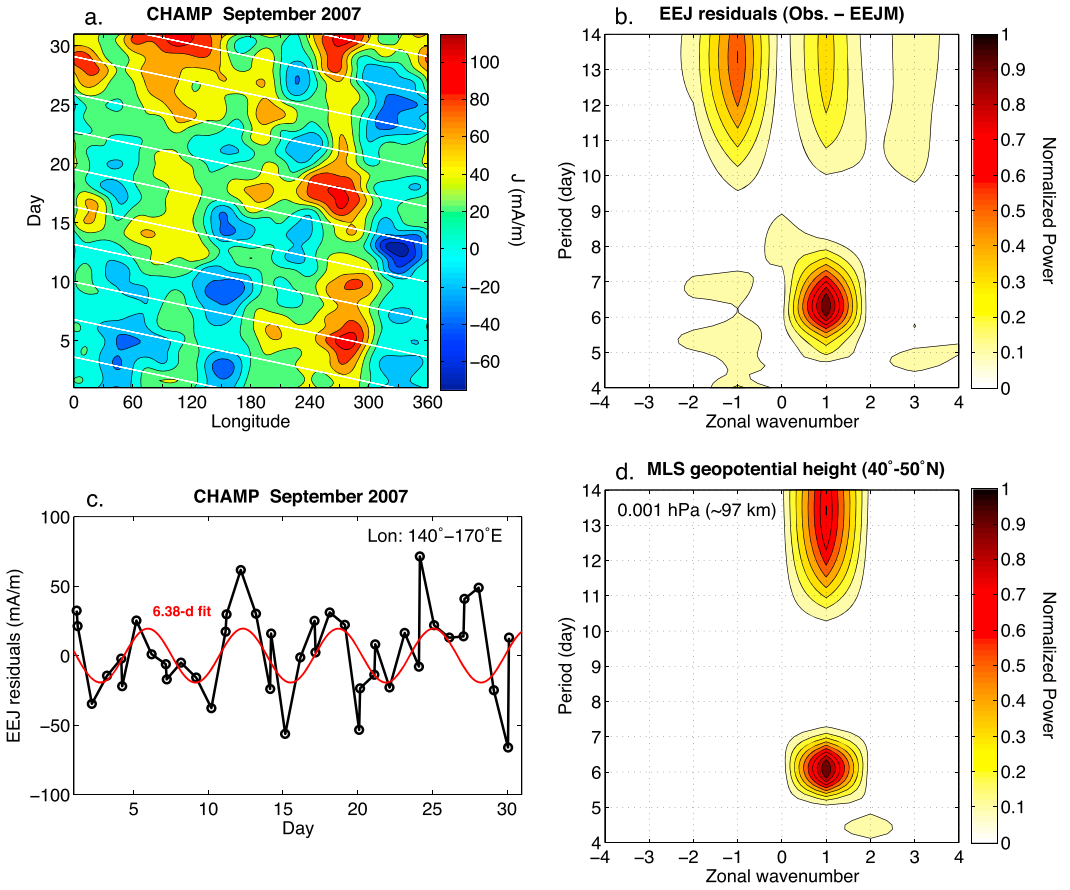

Figure 6. (a) Equatorial electrojet (EEJ) intensity during September 2007 as observed by the CHAMP satellite. The white lines represent the phase propagation of the 6.38-day wave with zonal wavenumber $s = 1$. (b) Period versus wavenumber (positive for westward propagating) spectrum for the residual equatorial electrojet intensity (observations minus equatorial electrojet model [EEJM] predictions). The spectral power is normalized to the peak value. (c) EEJ intensity at 140°–170°E longitudes, with the least squares fit of the 6.38-day Fourier curve. (d) Same as (b) except for the Microwave Limb Sounder (MLS) geopotential height at 0.001 hPa (~97-km height) in the latitude range 40°–50°N.

also studied by Merzlyakov et al. (2013). The wave spectra of the EEJ intensity (Figure 1e) and the geopotential height in the lower thermosphere (Figure 1g) bear a striking resemblance. The agreement holds not only for the peak spectrum ($T \sim 6$, $s = 1$) but also for the secondary peak ($T \sim 8$, $s = 1$). The results suggest that the short-term variability of the EEJ was under a significant influence of wave forcing from below.

As mentioned earlier, the quasi-6-day variation in the EEJ intensity observed during September 2006 is more evident at some longitudes than others. Figure 2 depicts perturbations of the EEJ intensity at two different longitude sectors: (top) at 180°–210°E and (bottom) at 30°–60°E. The red lines indicate the least squares fits of the 5.75-day Fourier component, which is the dominant period derived from the spectrum analysis (Figure 1e). The quasi-6-day variation is clearly seen at 180°–210°E, while it is far less clear at 30°–60°E. The amplitude of the 5.75-day Fourier component is 37.1 mA/m at 180°–210°E, more than 3 times as large as the amplitude at 30°–60°E (10.0 mA/m).

In order to see if such a strong longitudinal dependence exists in the quasi-6-day variation in the middle atmosphere, we compare in Figure 3 perturbations of the MLS geopotential height (top) at 180°–210°E and (bottom) at 30°–60°E. Following Riggin et al. (2006), a 4- to 7-day band-pass filter was used to extract the quasi-6-day variation. Enhanced activity of the quasi-6-day variation can be seen at both longitudes from the end of August 2006 to around 20 September 2006. The quasi-6-day variations extend from stratospheric heights to the lower thermosphere, consistent with earlier studies (e.g., Talaat et al., 2002). The difference in the amplitudes of the quasi-6-day variation between the two longitudes seems to be too small to explain the longitudinal difference found in the EEJ intensity. Therefore, the longitudinal dependence of the quasi-6-day

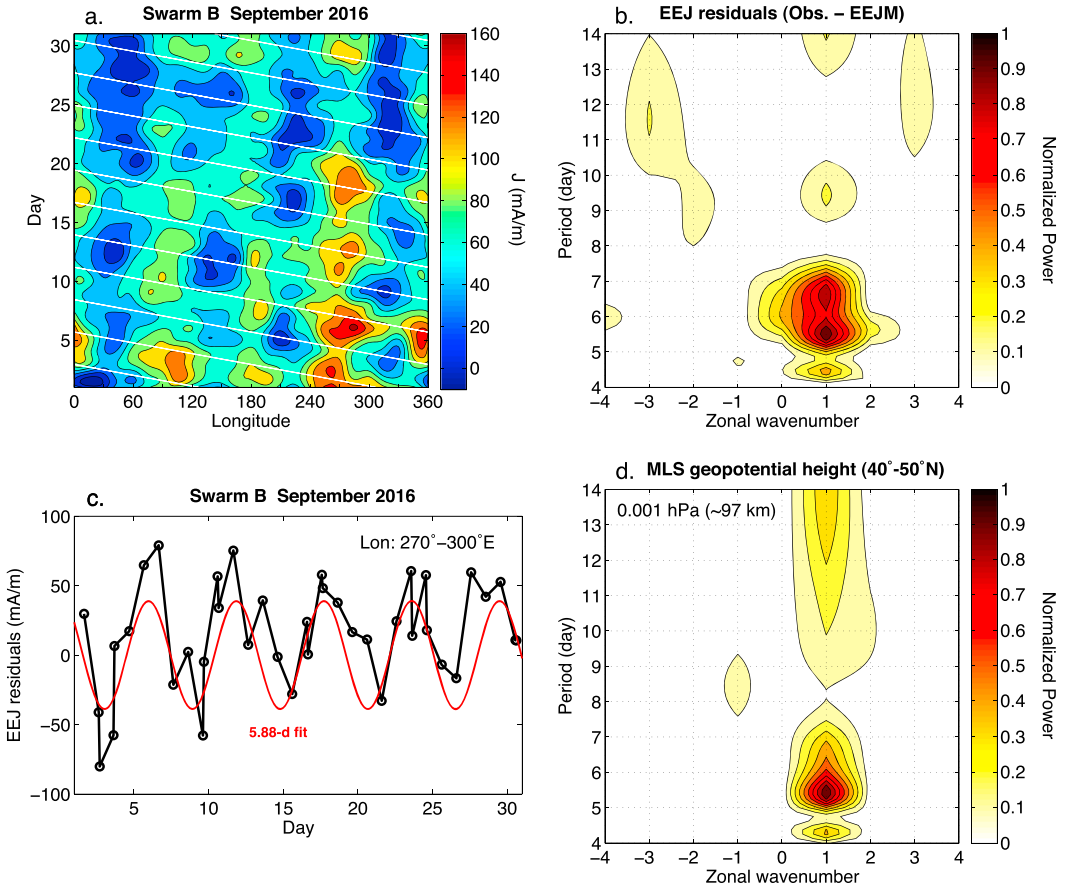

Figure 7. (a) Equatorial electrojet (EEJ) intensity during September 2016 as observed by the Swarm B satellite. The white lines represent the phase propagation of the 5.88-day wave with zonal wavenumber $s = 1$. (b) Period versus wavenumber (positive for westward propagating) spectrum for the residual equatorial electrojet intensity (observations minus equatorial electrojet model [EEJM] predictions). The spectral power is normalized to the peak value. (c) EEJ intensity at 270°–300°E longitudes, with the least squares fit of the 5.88-day Fourier curve. (d) Same as (b) except for the Microwave Limb Sounder (MLS) geopotential height at 0.001 hPa (~97-km height) in the latitude range 40°–50°N.

variation in the EEJ is considered to be due to the longitudinal dependence of the ionospheric response to wave forcing rather than due to the longitudinal dependence of wave forcing itself. The ionospheric response to wave forcing could be longitudinally dependent because of the zonally inhomogeneous distribution of the main geomagnetic field, which affects the local ionospheric conductivities and wind dynamo electric field.

4.2. May 2007 Event

Figure 4 shows the same variables as presented in Figure 1 except for May 2007. During this month, the CHAMP satellite flew over the afternoon sector of the equatorial ionosphere around 1200–1500 LT (Figure 4c). The overall longitudinal structure of the EEJ intensity (Figure 4a) is well reproduced by EEJM (Figure 4d), thus may be attributed to tidal effects. The spectrum for the EEJ intensity (Figure 4e) reveals the dominance of a westward propagating wave with the period $T = 5.63$ (± 0.29) days and zonal wavenumber $s = 1$. The corresponding wave spectrum can be found in the geopotential height in the lower thermosphere (Figure 4g). There is no apparent quasi-6-day variation in the *Kp* index (Figure 4b). More importantly, the spectrum of the *Kp* index sampled at the times of the CHAMP measurements (Figure 4f) is concentrated in the $s = 0$ component, and thus, the spectral peak of the EEJ intensity at $s = 1$ and $T = 5.63$ days (Figure 4e) is not a spurious signal due to zonally symmetric geomagnetic disturbances in the EEJ.

Figure 5 shows the quasi-6-day variations in the EEJ intensity at (top) 0°–30°E and (bottom) 180°–210°E longitudes. The quasi-6-day variation is clearly seen in the African longitude sector (0°–30°E) but hardly visible in the Pacific region (180°–210°E). The amplitude of the 5.63-day Fourier component is about twice as large in the African region than in the Pacific longitude sector. The longitudinal dependence is different from what

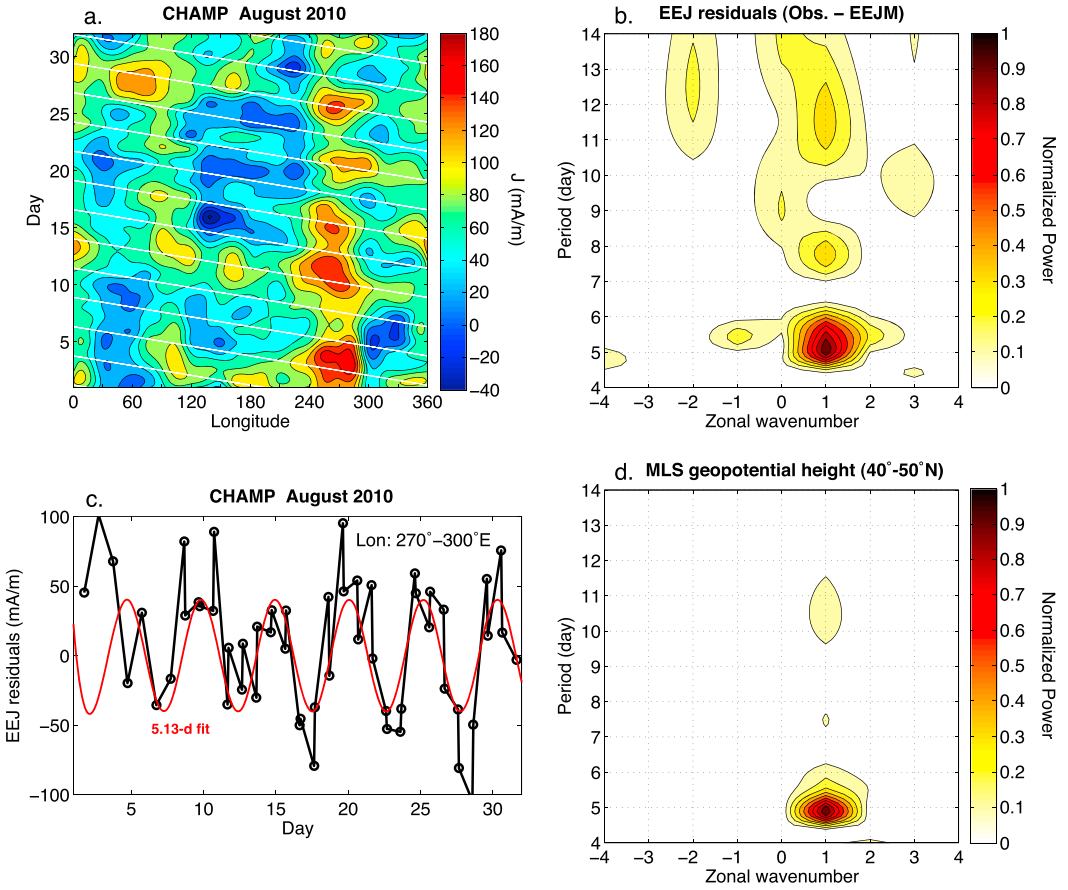

Figure 8. (a) Equatorial electrojet (EEJ) intensity during August 2010 as observed by the CHAMP satellite. The white lines represent the phase propagation of the 5.13-day wave with zonal wavenumber $s = 1$. (b) Period versus wavenumber (positive for westward propagating) spectrum for the residual equatorial electrojet intensity (observations minus equatorial electrojet model [EEJM] predictions). The spectral power is normalized to the peak value. (c) EEJ intensity at 270°–300°E longitudes, with the least squares fit of the 5.13-day Fourier curve. (d) Same as (b) except for the Microwave Limb Sounder (MLS) geopotential height at 0.001 hPa (~97-km height) in the latitude range 40°–50°N.

was observed during September 2006 (Figure 2), in which the quasi-6-day variation was most prominent in the Pacific longitude sector.

4.3. September 2007 Event

There was another event in 2007, which was observed during September, when the CHAMP satellite was in the afternoon sector around 1300–1600 LT. Figure 6 summarizes the observations during the event. Similar to the September 2006 event (Figure 1), the wave-4 pattern dominates the overall longitudinal structure (Figure 6a). The spectrum analysis of the EEJ intensity (Figure 6b) reveals a westward propagating $s = 1$ wave with the peak period of 6.38 (±0.27) days. The spectrum analysis of the MLS geopotential height data shows the spectral peak associated with the quasi-6-day wave (Figure 6d). The spectrum of the MLS geopotential height also shows a secondary peak around periods of 12–14 days with $s = 1$, which can be found in the spectrum of the EEJ intensity as well (Figure 6b). The quasi-6-day variation in the EEJ intensity was most evident in the western Pacific region (Figure 6c).

4.4. September 2016 Event

Figure 7 shows the quasi-6-day wave event observed by the Swarm B satellite during September 2016. During the event, the Swarm B satellite was in the morning sector around 0900–1200 LT. The spectrum of the EEJ intensity (Figure 7b) is dominated by westward propagating waves at periods of 4–7 days with zonal wavenumber $s = 1$. The peak period is found to be at 5.88 (±0.58) days. The MLS geopotential height measurements confirm the presence of the quasi-6-day wave in the lower thermosphere (Figure 7d). The power of $s = 1$ waves is relatively high at the period range 4–7 days, consistent with the spectral pattern for the EEJ

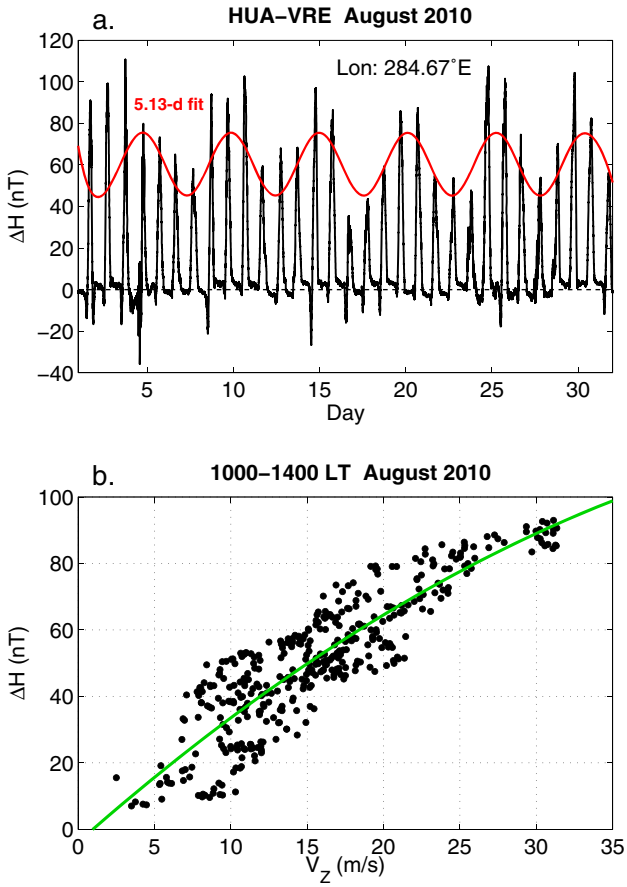

Figure 9. (a) ΔH (H at Huancayo [HUA] minus H at Villa Remedios [VRE]) as observed by ground-based magnetometers during August 2010. The red line is the least squares fit of the 5.13-day Fourier curve. (b) Scatter plot of ΔH and the equatorial vertical plasma drift velocity V_Z for August 2010. The green line indicates the second-order polynomial fit.

intensity (Figure 7b). The quasi-6-day variation in the EEJ intensity is depicted in Figure 7c for the American longitude sector (270° – 300°E).

4.5. August 2010 Event

Figure 8a shows the EEJ intensity during August 2010, when the CHAMP measurements were made around 1000 – 1300 LT. The spectral peak appears at the westward propagating component at the period $T = 5.13$ (± 0.24) days with a zonal wavenumber $s = 1$. The analysis of the MLS geopotential height also showed the spectral peak at $T \sim 5$ days and $s = 1$ (Figure 8d).

Figure 8c depicts the quasi-6-day variation of the EEJ intensity in the American longitude sector (270° – 300°E), where the amplitude of the quasi-6-day variation was relatively large. The 5.13-day Fourier component fits well to the measurements after 5 August 2010. During this event, ΔH data are also available from a pair of the magnetometers at Huancayo and Villa Remedios. As mentioned earlier, the parameter ΔH is directly comparable with the EEJ magnetic field measured by CHAMP and Swarm satellites (Manoj et al., 2006). We plot in Figure 9a ΔH during August 2010. The monthly average of the nighttime data between 2130 LT and 0230 LT, when the EEJ is effectively absent, was chosen to be the zero level. The ΔH values are generally positive during daytime owing to the eastward EEJ current. In Figure 9a, the daytime values of ΔH exhibit a quasi-6-day variation, after 5 August 2010. The red line in Figure 9a is the least squares fit of the 5.13-day Fourier component to the midday values of ΔH. A comparison with Figure 8c reveals that the phase of the quasi-6-day variation in ΔH is in agreement with that in the EEJ intensity derived from the CHAMP data. The amplitude of 5.13-day variation in ΔH at 1200 LT is 15.2 nT.

During the August 2010 event, the JULIA radar operated for several days for the measurement of the daytime vertical plasma drift velocity V_Z, which is a proxy of the zonal electric field. It turned out to be difficult

Table 1
Summary of the Quasi-6-Day Wave Events Examined in this Study

Event month	Peak EEJ period	Peak GPH period (40°–50°N)	Mean LT of EEJ measurement	Longitude of large EEJ
September 2006	5.75 (±0.10)	5.81 (±0.05)	12:08	180°–210°E
May 2007	5.63 (±0.29)	5.94 (±0.12)	13:49	0°–30°E
September 2007	6.38 (±0.28)	6.06 (±0.04)	14:27	150°–180°E
August 2010	5.13 (±0.24)	4.93 (±0.03)	11:35	135°–165°E
September 2016	5.88 (±0.58)	5.43 (±0.04)	10:16	270°–300°E

Note. Columns show, from the left to the right, the month of the quasi-6-day wave event, the period of the peak in the spectrum of the equatorial electrojet (EEJ) intensity, the period of the peak in the spectrum of the geopotential height, GPH (0.001 hPa, 40°–50°N), the mean local solar time (LT) for the equatorial electrojet measurements, the longitude sector where the quasi-6-day variation in the equatorial electrojet intensity is largest.

to determine the amplitude of the quasi-6-day variation directly from the discontinuous V_Z data. Thus, we first determine the quantitative relationship between V_Z and ΔH and then evaluate the amplitude of the quasi-6-day variation in V_Z based on the fact that the amplitude of the quasi-6-day variation in ΔH is 15.2 nT. In Figure 9b we compare the V_Z values observed between 1000 and 1400 LT with the corresponding ΔH values. The vertical plasma drift of 10 m/s is equivalent to the zonal electric field of approximately 0.23 mV/m at the Jicamarca location. Positive and negative values of V_Z correspond to eastward and westward electric fields, respectively. As can be seen in Figure 9b, there is a good correlation between V_Z from the JULIA radar and ΔH from the magnetometers. The green line in Figure 9b is the second-order polynomial fit, which is given as $V_Z = 2.3 \times 10^{-3} \Delta H^2 + 2.7 \times 10^{-2} \Delta H + 7.3$. The second-order term ΔH^2 is necessary because of the saturation of the EEJ intensity at high V_Z values. This saturation is known to be due to plasma instabilities in the equatorial ionosphere, which occur under the presence of a strong electric field (e.g., Alken & Maus, 2010). From the derived relationship between ΔH and V_Z, it is estimated that the amplitude of the quasi-6-day variation in V_Z, corresponding to 15.2 nT in ΔH at 1200 LT, is 5.9 m/s.

Gan et al. (2016), using the Thermosphere Ionosphere Mesosphere General Circulation Model, performed an idealized simulation of the ionospheric response to the quasi-6-day wave. It was demonstrated that a quasi-6-day variation in V_Z can be caused by wave forcing imposed at the model lower boundary at 30 km, which imitates the quasi-6-day planetary wave. They showed that the quasi-6-day variation of V_Z occurs mainly during presunrise times (±10 m/s at 0540 LT at 285°E) and the effect is much smaller during daytime (±1 m/s at 1100 LT at 285°E). Thus, the quasi-6-day variation of ±5.9 m/s observed in the midday values of V_Z is much larger than expected from previous knowledge.

5. Summary and Conclusions

It is well known that the EEJ intensity varies significantly from day to day. Previous studies suggested that the atmospheric waves that propagate to the ionosphere from below could be a cause of such variability (Kawano-Sasaki & Miyahara, 2008; Yamazaki et al., 2014). However, it has been unclear which waves play a role and how much they affect the EEJ. Recent simulation studies (Gan et al., 2016, 2017) pointed to the possible influence of the quasi-6-day wave on the equatorial ionospheric electrodynamics.

We have examined the events, where the EEJ intensity derived from the magnetic field measurements by CHAMP and Swarm satellites shows an oscillatory variation with a period of ~6 days at a fixed longitude. During such events, the spectrum of the EEJ intensity is found to be dominated by a westward propagating wave with the period of approximately 6 days and zonal wavenumber 1. We attribute this to the electric field modulation by the quasi-6-day wave that directly penetrates into the *E* region ionosphere. Previous studies based on ground measurements had difficulties in identifying the quasi-6-day wave in the EEJ due to limited spatial coverage, which we have overcome with the satellite data. Moreover, using the geopotential height data from the Aura satellite, we have confirmed the presence of the quasi-6-day planetary wave in the lower thermosphere for all the events.

Table 1 gives a summary of the five events we examined in this study. It should be noted that Table 1 is not necessarily the complete list of the events where the EEJ was under the influence of the quasi-6-day wave

during the period of our investigation (i.e., August 2000 to August 2010 and December 2013 to April 2017). This is because our study was limited to the months when the satellite measurements were made at local times around 1200 LT. As can be seen in Table 1, three out of five events are observed in September. This seems to be consistent with previous studies, which found that the amplitude of the quasi-6-day wave in the MLT region shows a semiannual variation with equinoctial maxima (e.g., H.-L. Liu et al., 2004; Pancheva et al., 2010). More studies would be required to establish the seasonal dependence of the quasi-6-day wave influence on the ionosphere.

Table 1 also shows that the peak period of the quasi-6-day wave component in the EEJ intensity (second column) is consistent with the dominant wave period observed in the lower thermosphere (third column). This is another piece of evidence supporting a physical link between the quasi-6-day planetary wave and EEJ variability.

The quasi-6-day variation in the EEJ intensity has been observed to be more prominent at some longitudes than others. This behavior deviates from the effect of a westward propagating wave with zonal wavenumber 1 on the zonally uniform ionosphere, which would cause quasi-6-day variations at different longitudes with different phases but with the same amplitude. We suggest that the longitudinal dependence of the quasi-6-day variation in the EEJ is due to the longitudinal dependence of the ionosphere, rather than the longitudinal dependence of wave forcing. Longitudinal sectors, where the amplitude of the quasi-6-day variation in the EEJ is largest, are shown in Table 1. There is no evidence of consistent longitudinal dependence for different events. Numerical studies would be necessary to elucidate the mechanism for the observed longitudinal dependence.

At selected longitudes, the amplitude of the quasi-6-day variation in the EEJ intensity is as large as 40 mA/m, which corresponds to the amplitude of 5.9 m/s in the equatorial vertical plasma drift velocity at noontime, as evaluated for the August 2010 event. This is much larger than previously predicted (~1 m/s at 1100 LT) from an idealized simulation by Gan et al. (2016). More theoretical work is needed for a better understanding of the ionospheric response to the quasi-6-day wave. Especially, an assessment based on a whole atmosphere model (Akmaev, 2011) for actual quasi-6-day wave events is desirable.

Acknowledgments
The CHAMP satellite mission has been operated by German Research Centre for Geosciences (GFZ) and German Aerospace Center (DLR, former DARA). CHAMP data can be downloaded from isdc.gfz-potsdam.de/champ-isdc. The Swarm satellite constellation mission is operated by the European Space Agency (ESA). Swarm data are accessible through earth.esa.int/swarm. The equatorial electrojet model (EEJM version 2.0) can be downloaded from the CIRES website at geomag.colorado.edu/equatorial-electrojet-model-eejm2.html. The results presented in this paper partly rely on the magnetic data collected at Huancayo and Villa Remedios. We acknowledge the Instituto Geofisico del Peru (IGP) and INTERMAGNET (www.intermagnet.org/) for the operation of the Huancayo magnetometer and the distribution of the Huancayo data, respectively. We also acknowledge Universidad Mayor de San Andres (UMSA) and GFZ for the operation of the magnetometer at Villa Remedios. Our results also partly rely on the JULIA radar data from the Jicamarca Observatory. The Jicamarca Observatory is a facility of IGP operated with support from the NSF grant AGS-905448 through the Cornell University. The radar data used are available at jro.igp.gob.pe/madrigal. We thank the Aura MLS team at Jet Propulsion Laboratory for providing the geopotential height data. The MLS geopotential height data used in this study are available at disc.gsfc.nasa.gov. The *Kp* index was provided by GFZ, available at www.gfz-potsdam.de/en/kp-index/. C. S. and J. M. were partly supported by the Priority Program 1788 "Dynamic Earth" of Deutsche Forschungsgemeinschaft (DFG). Y. Y. was supported by the Humboldt Research Fellowship for Experienced Researchers from the Alexander von Humboldt Foundation.

References

Akmaev, R. A. (2011). Whole atmosphere modeling: Connecting terrestrial and space weather. *Reviews of Geophysics*, *49*, RG4004. https://doi.org/10.1029/2011RG000364

Alken, P. (2009). Modeling equatorial ionospheric currents and electric fields from satellite magnetic field measurements (PhD thesis). University of Colo. at Boulder, Boulder.

Alken, P., & Maus, S. (2007). Spatio-temporal characterization of the equatorial electrojet from CHAMP, Ørsted, and SAC-C satellite magnetic measurements. *Journal of Geophysical Research*, *112*, A09305. https://doi.org/10.1029/2007JA012524

Alken, P., & Maus, S. (2010). Relationship between the ionospheric eastward electric field and the equatorial electrojet. *Geophysical Research Letters*, *37*, L04104. https://doi.org/10.1029/2009GL041989

Alken, P., Maus, S., Vigneron, P., Sirol, O., & Hulot, G. (2013). Swarm SCARF equatorial electric field inversion chain. *Earth, Planets and Space*, *65*(11), 1309–1317. https://doi.org/10.5047/eps.2013.09.008

Anderson, D., Anghel, A., Chau, J., & Veliz, O. (2004). Daytime vertical E × B drift velocities inferred from ground-based magnetometer observations at low latitudes. *Space Weather*, *2*, S11001. https://doi.org/10.1029/2004SW000095

Chau, J. L., & Kudeki, E. (2006). Statistics of 150-km echoes over Jicamarca based on low-power VHF observations. *Annales de Geophysique*, *24*, 1305–1310.

Chulliat, A., Vigneron, P., & Hulot, G. (2016). First results from the Swarm dedicated ionospheric field inversion chain. *Earth, Planets and Space*, *68*, 1–18. https://doi.org/10.1186/s40623-016-0481-6

Day, K. A., Hibbins, R. E., & Mitchell, N. J. (2011). Aura MLS observations of the westward-propagating $s = 1$, 16-day planetary wave in the stratosphere, mesosphere and lower thermosphere. *Atmospheric Chemistry and Physics*, *11*, 4149–4161. https://doi.org/10.5194/acp-11-4149-2011

Du, J., & Stening, R. J. (1999). Simulating the ionospheric dynamo—II. Equatorial electric fields. *Journal of Atmospheric and Solar-Terrestrial Physics*, *61*, 925–940.

Elhawary, R., & Forbes, J. M. (2016). Planetary wave variability of Sq currents. *Journal of Geophysical Research: Space Physics*, *121*, 11,316–11,332. https://doi.org/10.1002/2016JA023242

England, S. L., Maus, S., Immel, T. J., & Mende, S. B. (2006). Longitudinal variation of the E-region electric fields caused by atmospheric tides. *Geophysical Research Letters*, *33*, L21105. https://doi.org/10.1029/2006GL027465

Fang, T.-W., Akmaev, R., Fuller-Rowell, T., Wu, F., Maruyama, N., & Millward, G. (2013). Longitudinal and day-to-day variability in the ionosphere from lower atmosphere tidal forcing. *Geophysical Research Letters*, *40*, 2523–2528. https://doi.org/10.1002/grl.50550

Fejer, B. G., Blanc, M., & Richmond, A. D. (2017). Post-storm middle and low-latitude ionospheric electric fields effects. *Space Science Reviews*, *206*, 407–429. https://doi.org/10.1007/s11214-016-0320-x

Forbes, J. M. (1995). Tidal and planetary waves (a tutorial). In R. M. Johnson & T. L. Killeen (Eds.), *The upper mesosphere and lower thermosphere: A review of experiment and theory, Geophysical Monograph Series* (Vol. 87, pp. 67–87). Washington, DC: American Geophysical Union.

Forbes, J. M., & Zhang, X. (2015). Quasi-10-day wave in the atmosphere. *Journal of Geophysical Research: Atmospheres*, *120*, 11,079–11,089. https://doi.org/10.1002/2015JD023327

Forbes, J. M., & Zhang, X. (2017). The quasi-6 day wave and its interactions with solar tides. *Journal of Geophysical Research: Space Physics*, *122*, 4764–4776. https://doi.org/10.1002/2017JA023954

Forbes, J. M., Zhang, X., Bruinsma, S., & Oberheide, J. (2013). Lunar semidiurnal tide in the thermosphere under solar minimum conditions. *Journal of Geophysical Research: Space Physics*, *118*, 1788–1801. https://doi.org/10.1029/2012JA017962

Forbes, J. M., Zhang, X., Maute, A., & Hagan, M. E. (2018). Zonally-symmetric oscillations of the thermosphere at planetary-wave periods. *Journal of Geophysical Research: Space Physics*, *123*. https://doi.org/10.1002/2018JA025258

Forbes, J. M., Zhang, X., Palo, S., Russell, J., Mertens, C. J., & Mlynczak, M. (2008). Tidal variability in the ionospheric dynamo region. *Journal of Geophysical Research*, *113*, A02310. https://doi.org/10.1029/2007JA012737

Friis-Christensen, E., Lühr, H., & Hulot, G. (2006). Swarm: A constellation to study the Earth's magnetic field. *Earth, Planets and Space*, *58*, 351–358.

Friis-Christensen, E., Lühr, H., Knudsen, D., & Haagmans, R. (2008). Swarm—An Earth observation mission investigating geospace. *Advances in Space Research*, *41*, 210–216. https://doi.org/10.1016/j.asr.2006.10.008

Fuller-Rowell, T., Wu, F., Akmaev, R., Fang, T.-W., & Araujo-Pradere, E. (2010). A whole atmosphere model simulation of the impact of a sudden stratospheric warming on thermosphere dynamics and electrodynamics. *Journal of Geophysical Research*, *115*, A00G08. https://doi.org/10.1029/2010JA015524

Gan, Q., Oberheide, J., Yue, J., & Wang, W. (2017). Short-term variability in the ionosphere due to the nonlinear interaction between the 6 day wave and migrating tides. *Journal of Geophysical Research: Space Physics*, *122*, 8831–8846. https://doi.org/10.1002/2017JA023947

Gan, Q., Wang, W., Yue, J., Liu, H., Chang, L. C., Zhang, S., et al. (2016). Numerical simulation of the 6 day wave effects on the ionosphere: Dynamo modulation. *Journal of Geophysical Research: Space Physics*, *121*, 10,103–10,116. https://doi.org/10.1002/2016JA022907

Gu, S., Li, T., Dou, X., Wu, Q., Mlynczak, M. G., & Russell, J. M. (2013). Observations of quasi-two-day wave by TIMED/SABER and TIMED/TIDI. *Journal of Geophysical Research: Atmospheres*, *118*, 1624–1639. https://doi.org/10.1002/jgrd.50191

Gu, S. Y., Liu, H. L., Li, T., Dou, X. K., Wu, Q., & Russell, J. M. (2014). Observation of the neutral-ion coupling through 6 day planetary wave. *Journal of Geophysical Research: Space Physics*, *119*, 10,376–10,383. https://doi.org/10.1002/2014JA020530

Gurubaran, S., Dhanya, R., Sathiskumar, S., & Patil, P. T. (2011). A case study of tidal and planetary wave coupling in the equatorial atmosphere-ionosphere system over India: Preliminary results. In M. A. Abdu, D. Pancheva, & B. Archana (Eds.), *Aeronomy of the Earth's Atmosphere and Ionosphere* (pp. 177–187). New York: Springer.

Hirooka, T., & Hirota, I. (1984). Normal mode Rossby waves observed in the upper stratosphere. Part 2: Second symmetric modes of zonal wavenumbers 1 and 2. *Journal of the Atmospheric Sciences*, *41*, 536–548.

Hirooka, T. (2000). Normal mode Rossby waves as revealed by UARS/ISAMS observations. *Journal of the Atmospheric Sciences*, *57*, 1277–1285.

Hysell, D. L., Chau, J. L., & Fesen, C. G. (2002). Effects of large horizontal winds on the equatorial electrojet. *Journal of Geophysical Research*, *107*(A8), 1214. https://doi.org/10.1029/2001JA000217

Hysell, D. L., Larsen, M. F., & Woodman, R. F. (1997). JULIA radar studies of electric fields in the equatorial electrojet. *Geophysical Research Letters*, *24*, 1687–1690.

Jarvis, M. J. (2006). Planetary wave trends in the lower thermosphere—Evidence for 22-year solar modulation of the quasi 5-day wave. *Journal of Atmospheric and Solar-Terrestrial Physics*, *68*(17), 1902–1912. https://doi.org/10.1016/j. jastp.2006.02.014

John, S. R., & Kumar, K. K. (2016). Global normal mode planetary wave activity: A study using TIMED/SABER observations from the stratosphere to the mesosphere-lower thermosphere. *Climate Dynamics*, *47*, 3863–3881. https://doi.org/10.1007/s00382-016-3046-2

Kawano-Sasaki, K., & Miyahara, S. (2008). A study on three-dimensional structures of the ionospheric dynamo currents induced by the neutral winds simulated by the Kyushu-GCM. *Journal of Atmospheric and Solar-Terrestrial Physics*, *70*, 1549–1562.

Laundal, K. M., & Richmond, A. D. (2017). Magnetic coordinate systems. *Space Science Reviews*, *206*, 27–59. https://doi.org/10.1007/s11214-016-0275-y

Laštovička, J. (2006). Forcing of the ionosphere by waves from below. *Journal of Atmospheric and Solar-Terrestrial Physics*, *68*, 479–497.

Lieberman, R. S., Riggin, D. M., Franke, S. J., Manson, A. H., Meek, C., Nakamura, T., et al. (2003). The 6.5-day wave in the mesosphere and lower thermosphere: Evidence for baroclinic/barotropic instability. *Journal of Geophysical Research*, *108*(D20), 4640. https://doi.org/10.1029/2002JD003349

Limpasuvan, V., Wu, D. L., Schwartz, M. J., Waters, J. W., Wu, Q., & Killeen, T. L. (2005). The two-day wave in EOS MLS temperature and wind measurements during 2004–2005 winter. *Geophysical Research Letters*, *32*, L17809. https://doi.org/10.1029/2005GL023396

Liu, G., Immel, T. J., England, S. L., Kumar, K. K., & Ramkumar, G. (2010). Temporal modulations of the longitudinal structure in F2 peak height in the equatorial ionosphere as observed by COSMIC. *Journal of Geophysical Research*, *115*, A04303. https://doi.org/10.1029/2009JA014829

Liu, H.-L. (2016). Variability and predictability of the space environment as related to lower atmosphere forcing. *Space Weather*, *14*, 634–658. https://doi.org/10.1002/2016SW001450

Liu, H.-L., Talaat, E. R., Roble, R. G., Lieberman, R. S., Riggin, D. M., & Yee, J.-H. (2004). The 6.5-day wave and its seasonal variability in the middle and upper atmosphere. *Journal of Geophysical Research*, *109*, D21112. https://doi.org/10.1029/2004JD004795

Longuet-Higgins, M. S. (1968). The eigenfunctions of Laplaces tidal equations over a sphere. *Philosophical Transactions of the Royal Society A*, *262*, 511–607. https://doi.org/10.1098/rsta.1968.0003

Lühr, H., & Manoj, C. (2013). The complete spectrum of the equatorial electrojet related to solar tides: CHAMP observations. *Annales de Geophysique*, *31*, 1315–1331. https://doi.org/10.5194/angeo-31-1315-2013

Lühr, H., Rother, M., Häusler, K., Alken, P., & Maus, S. (2008). The influence of nonmigrating tides on the longitudinal variation of the equatorial electrojet. *Journal of Geophysical Research*, *113*, A08313. https://doi.org/10.1029/2008JA013064

Manoj, C., Lühr, H., Maus, S., & Nagarajan, N. (2006). Evidence for short spatial correlation lengths of the noontime equatorial electrojet inferred from a comparison of satellite and ground magnetic data. *Journal of Geophysical Research*, *111*, A11312. https://doi.org/10.1029/2006JA011855

Matzka, J., Ricaldi, E., & Miranda, P. (2018). Preliminary minute mean values of geomagnetic observatory Villa Remedios, Bolivia, August 2010. V. 1.0. GFZ Data Services. https://doi.org/10.5880/GFZ.2.3.2018.004

McDonald, A. J., Hibbins, R. E., & Jarvis, M. J. (2011). Properties of the quasi 16 day wave derived from EOS MLS observations. *Journal of Geophysical Research*, *116*, D06112. https://doi.org/10.1029/2010JD014719

Merzlyakov, E. G., Solovjova, T. V., & Yudakov, A. A. (2013). The interannual variability of a 5–7 day wave in the middle atmosphere in autumn from ERA product data, Aura MLS data, and meteor wind data. *Journal of Atmospheric and Solar-Terrestrial Physics*, *102*, 281–289. https://doi.org/10.1016/j.jastp.2013.06.008

Meyer, C. K., & Forbes, J. M. (1997). A 6.5-day westward propagating planetary wave: Origin and characteristics. *Journal of Geophysical Research*, *102*, 26,173–26,178.

Miyoshi, Y. (1999). Numerical simulation of the 5-day and 16-day waves in the mesopause region. *Earth, Planets and Space*, *51*, 763–772.
Miyoshi, Y., & Hirooka, T. (1999). A numerical experiment of excitation of the 5-day wave by a GCM. *Journal of the Atmospheric Sciences*, *56*, 1698–1707.
Moudden, Y., & Forbes, J. M. (2014). Quasi-two-day wave structure, interannual variability, and tidal interactions during the 2002–2011 decade. *Journal of Geophysical Research: Atmospheres*, *119*, 2241–2260. https://doi.org/10.1002/2013JD020563
Newell, P. T., & Gjerloev, J. W. (2011). Evaluation of SuperMAG auroral electrojet indices as indicators of substorms and auroral power. *Journal of Geophysical Research*, *116*, A12211. https://doi.org/10.1029/2011JA016779
Oberheide, J., Shiokawa, K., Gurubaran, S., Ward, W. E., Fujiwara, H., Kosch, M. J., et al. (2015). The geospace response to variable inputs from the lower atmosphere: A review of the progress made by Task Group 4 of CAWSES-II. *Progress in Earth and Planetary Science*, *2*, 2. https://doi.org/10.1186/s40645-014-0031-4
Pancheva, D., Mukhtarov, P., Andonov, B., & Forbes, J. M. (2010). Global distribution and climatological features of the 5–6-day planetary waves seen in the SABER/TIMED temperatures (2002–2007). *Journal of Atmospheric and Solar-Terrestrial Physics*, *72*, 26–37. https://doi.org/10.1016/j.jastp.2009.10.005
Pancheva, D., Mukhatrov, P., Mitchell, N., Fritts, D., Riggin, D., Takahashi, H., et al. (2008). Planetary wave coupling (5–6-day waves) in the low latitude atmosphere-ionosphere system. *Journal of Atmospheric and Solar-Terrestrial Physics*, *70*, 101–122.
Parish, H. F., Forbes, J. M., & Kamalabadi, F. (1994). Planetary wave and solar emission signatures in the equatorial electrojet. *Journal of Geophysical Research*, *99*, 355–368. https://doi.org/10.1029/93JA02096
Pedatella, N. M., Liu, H.-L., Richmond, A. D., Maute, A., & Fang, T.-W. (2012). Simulations of solar and lunar tidal variability in the mesosphere and lower thermosphere during sudden stratosphere warmings and their influence on the low-latitude ionosphere. *Journal of Geophysical Research*, *117*, A08326. https://doi.org/10.1029/2012JA017858
Pedatella, N. M., Oberheide, J., Sutton, E. K., Liu, H.-L., Anderson, J. L., & Raeder, K. (2016). Short-term nonmigrating tide variability in the mesosphere, thermosphere, and ionosphere. *Journal of Geophysical Research: Space Physics*, *121*, 3621–3633. https://doi.org/10.1002/2016JA022528
Ramkumar, T. K., Gurubaran, S., & Rajaram, R. (2009). Mesospheric planetary wave signatures in the equatorial electrojet. *Journal of Geophysical Research*, *114*, A03309. https://doi.org/10.1029/2007JA012935
Rastogi, R. G., & Klobuchar, J. A. (1990). Ionospheric electron content within the equatorial F_2 layer anomaly belt. *Journal of Geophysical Research*, *95*(A11), 19,045–19,052. https://doi.org/10.1029/JA095iA11p19045
Reigber, C., Lühr, H., & Schwintzer, P. (2002). CHAMP mission status. *Advances in Space Research*, *30*, 129–134.
Richmond, A. D. (1973). Equatorial electrojet—I. Development of a model including winds and instabilities. *Journal of Atmospheric and Solar-Terrestrial Physics*, *35*, 1083–1103.
Richmond, A. D., & Maute, A. (2014). Ionospheric electrodynamics modeling. In J. Huba, R. Schunk, & G. Khazanov (Eds.), *Modeling the ionosphere-thermosphere system*. Chichester, UK: John Wiley. https://doi.org/10.1002/9781118704417.ch6
Riggin, D. M., Liu, H.-L., Lieberman, R. S., Roble, R. G., Russell III, J. M., Mertens, C. J., et al. (2006). Observations of the 5-day wave in the mesosphere and lower thermosphere. *Journal of Atmospheric and Solar-Terrestrial Physics*, *68*, 323–339.
Salby, M. L. (1981). The 2-day wave in the middle atmosphere: Observations and theory. *Journal of Geophysical Research*, *86*(C10), 9654–9660. https://doi.org/10.1029/JC086iC10p09654
Schwartz, M. J., Lambert, A., Manney, G. L., Read, W. G., Livesey, N. J., & Froidevaux, L. (2008). Validation of the Aura Microwave Limb Sounder temperature and geopotential height measurements. *Journal of Geophysical Research*, *113*, D15S11. https://doi.org/10.1029/2007JD008783
Stening, R. J. (1995). What drives the equatorial electrojet. *Journal of Atmospheric and Terrestrial Physics*, *57*, 1117–1128.
Stolle, C., Manoj, C., Lühr, H., Maus, S., & Alken, P. (2008). Estimating the daytime equatorial ionization anomaly strength from electric field proxies. *Journal of Geophysical Research*, *113*, A09310. https://doi.org/10.1029/2007JA012781
Takahashi, H., Wrasse, C. M., Pancheva, D., Abdu, M. A., Batista, I. S., Lima, L. M., et al. (2006). Signatures of 3–6 day planetary waves in the equatorial mesosphere and ionosphere. *Annales de Geophysique*, *24*, 3343–3350.
Takeda, M. (2002). Features of global geomagnetic Sq field from 1980 to 1990. *Journal of Geophysical Research*, *107*(A9), 1252. https://doi.org/10.1029/2001JA009210
Talaat, E. R., Yee, J. H., & Zhu, X. (2001). Observations of the 6.5-day wave in the mesosphere and lower thermosphere. *Journal of Geophysical Research*, *106*, 20,715–20,723.
Talaat, E. R., Yee, J.-H., & Zhu, X. (2002). The 6.5-day wave in the tropical stratosphere and mesosphere. *Journal of Geophysical Research*, *107*(D12), 4133. https://doi.org/10.1029/2001JD000822
Truskowski, A. O., Forbes, J. M., Zhang, X., & Palo, S. E. (2014). New perspectives on thermosphere tides—1. Lower thermosphere spectra and seasonal-latitudinal structures. *Earth, Planets and Space*, *66*, 136. https://doi.org/10.1186/s40623-014-0136-4
Untiedt, J. (1967). A model of the equatorial electrojet involving meridional currents. *Journal of Geophysical Research*, *72*(23), 5799–5810. https://doi.org/10.1029/JZ072i023p05799
Xiong, C., Lühr, H., & Fejer, B. G. (2016). The response of equatorial electrojet, vertical plasma drift, and thermospheric zonal wind to enhanced solar wind input. *Journal of Geophysical Research: Space Physics*, *121*, 5653–5663. https://doi.org/10.1002/2015JA022133
Yamada, Y. (2002). 2-day, 3-day, and 5–6-day oscillations of the geomagnetic field detected by principal component analysis. *Earth, Planets and Space*, *54*, 379–392.
Yamazaki, Y., & Kosch, M. J. (2015). The equatorial electrojet during geomagnetic storms and substorms. *Journal of Geophysical Research: Space Physics*, *120*, 2276–2287. https://doi.org/10.1002/2014JA020773
Yamazaki, Y., & Maute, A. (2017). Sq and EEJ—A review on the daily variation of the geomagnetic field caused by ionospheric dynamo currents. *Space Science Reviews*, *206*, 299–405. https://doi.org/10.1007/s11214-016-0282-z
Yamazaki, Y., Richmond, A. D., Maute, A., Liu, H.-L., Pedatella, N., & Sassi, F. (2014). On the day-to-day variation of the equatorial electrojet during quiet periods. *Journal of Geophysical Research: Space Physics*, *119*, 6966–6980. https://doi.org/10.1002/2014JA020243
Yamazaki, Y., Stolle, C., Matzka, J., Siddiqui, T. A., Lühr, H., & Alken, P. (2017). Longitudinal variation of the lunar tide in the equatorial electrojet. *Journal of Geophysical Research: Space Physics*, *122*, 12,445–12,463. https://doi.org/10.1002/2017JA024601
Yiğit, E., & Medvedev, A. S. (2015). Internal wave coupling processes in Earth's atmosphere. *Advances in Space Research*, *55*, 983–1003.
Waters, J. W., Froidevaux, L., Harwood, R. S., Jarnot, R. F., Pickett, H. M., Read, W. G., et al. (2006). The Earth Observing System Microwave Limb Sounder (EOS MLS) on the Aura satellite. *IEEE Transactions on Geoscience and Remote Sensing*, *44*, 1075–1092.
Wu, D. L., Hays, P. B., & Skinner, W. R. (1994). Observations of the 5-day wave in the mesosphere and lower thermosphere. *Geophysical Research Letters*, *21*, 2733–2736.